Chemical selection for the calibration of general-purposed electronic noses based on Silhouette coefficients

Zhiyuan Wu, Fengchun Tian*, *Member*, *IEEE*, James A. Covington*, *Member*, *IEEE*, Hantao Li, Siyuan Deng

***Abstract*—Sensor drift is often application-dependent and results in a reduction in the overall long-term performance of electronic noses. Even with drift compensation it is remains challenging to transfer these models to other application scenarios. In order to remedy this deficiency, different/generic chemicals are needed to provide a general-purpose calibration approach that can be applied to a wide range of electronic noses. In this paper, we investigated a method to identify these chemicals based on four criteria (universality, safety, sensibility, and differentiation). This concept was tested on an in-house electronic nose comprising of 37 gas sensors and four environmental sensors combined with an automatic gas acquisition system. Fourteen different volatile compounds were tested over four months. The Silhouette coefficient was used to evaluate the extent of the sensor drift. Six different chemicals (acetone, alcohol, ethyl acetate, tetrahydrofuran, acetaldehyde, and n-hexane) were finally selected as the most appropriate to calibrate our E-nose. We believe our research may motivate the design of a reasonable chemical selection method for the calibration of general-purpose E-noses.**

***Index Terms*—Electronic nose, Calibration chemical selection, Volatile organic compounds, Silhouette coefficient.**

I. INTRODUCTION

ELECTRONIC noses (E-noses) are systems that attempt to mimic the mammalian olfactory system and are used extensively to identify or quantify complex odours. Typically, an E-nose consists of three components: a gas sensor array, a data pre-processing unit, and a pattern recognition module. E-noses have a number of advantages over more traditional analytical instruments, including simpler operation and providing almost real time results. For this reason, E-noses have been applied to medical applications [1], environmental testing [2], food engineering [3]-[4], medicine quality evaluation [5] and public security [6].

The progressive and unpredictable variation of the sensory signal, i.e., the sensor drift [7], has long been recognized as one of the most significant issues facing E-noses. This phenomenon degrades the stability of E-nose systems and can make its pattern recognition modules outdated [8]. The sensor drift stems from a variety of factors including sensor aging [9], contamination of the sensitive material [10] and as a result of thermal cycling through a variety of normal operations [11]. A further issue, beyond the above, is that exposure to different chemicals can lead to different sensor drift directions, making the calibration of the E-nose particularly challenging [9], [12]. This makes it difficult to objectively identify the drift mechanism and almost impossible to design appropriate strategies for correcting drift from unknown origins. Consequently, considering the compensation of drift, some researchers have concentrated on physical improvements on the gas sensor itself [13], [14], and others on algorithms [15]-[17]. Nevertheless, the drift mechanism is complex and inevitable, and so sensor drift has been identified as one of the primary obstacles to the mass production of E-noses [12].

Most existing researches rely on algorithms to compensate for sensor drift without systematic considering on the calibration or the impact of chemicals on the sensor drift [18]. Sensor drift is application-dependent, and experiences in drift resistance applied to one scenario are challenging to transfer to another.

In order to try and remedy this deficiency, different types of chemicals should be analyzed and screened to select the most representative ones for calibration of the majority of E-noses. For instance, Vergara *et al*. [19] collected an extensive dataset for six distinct volatile organic compounds (VOCs) over three years under strictly controlled operating conditions using an array of sixteen metal-oxide gas sensors (MOS) [20]-[22].

The majority of datasets used for E-nose calibration are from either publicly available datasets or from specific application scenarios wherein the selection of calibration chemical varies [23]-[26]. For example, Zhang *et al*. [23] proposed a unified framework called ‘domain adaptation extreme learning

This work is founded by the Natural Science Foundation of China (No. 62171066). (Corresponding author: Fengchun Tian, James A. Covington.)

Zhiyuan Wu, Hantao Li and Siyuan Deng are with the School of Microelectronic and Communication Engineering, Chongqing University, Chongqing, 400044, China (e-mail: wuzhiyuan@cqu.edu.cn; hantaoli@cqu.edu.cn; 20183669@cqu.edu.cn).

Fengchun Tian is with the School of Microelectronic and Communication Engineering, Chongqing University, Chongqing; Chongqing Key Laboratory of Bio-perception and Intelligent Information Processing, Chongqing, 400044, China (e-mail: fengchuntian@cuq.edu.cn).

James A. Covington is with the School of Engineering, University of Warwick, Coventry, CV47AL, UK (e-mail: J.A.Covington@warwick.ac.uk).

machine' (DAELM) for drift compensation [19]. Padilla *et al*. [15] presented a dataset containing measurements of three analytes (ammonia, propionic acid, and n-butanol) using an array of seventeen conductive polymer gas sensors. Liang *et al*. [22] provided a dataset composed of measurements of six analytes (ethanol, ethylene, ammonia, acetaldehyde, acetone, toluene, n-propanol) using an array of sixteen MOS sensors. However, there are currently no unified criteria for the selection of calibration chemicals. The closest is where E-nose companies have defined test chemicals for system evaluation purposes, though this data is not in the public domain.

In addition to academic research, we can consider German, European and American requirements of odour detection instruments and the composition of common workplace chemicals [27]-[32]. The German standard VDI/VDE 3518 specifies 57 different chemical alternatives for use with gas sensors in various workplaces [27]. Compared with VDI/VDE 3518, the NIOSH Pocket Guide to Chemical Hazards standard does not contain bromine, isobutanol, dibutylamine, methanol, triethylamine, vanillin and mixed xylene [30]. Likewise, there are no recommended chemicals in these international standards for E-nose calibration [27]-[32].

Here, we report on the use of a self-developed, general-purpose E-nose to systematically study the chemical selection for calibration and to quantify the drift for different chemicals. Our E-nose system has an array of sensors 41 sensors with 37 gas sensors (electrochemical, MOS, PID, MEMS, etc.) and four environmental sensors (temperature & humidity, and barometric pressure). The sources and compositions of volatile compounds in various environments were investigated, and 14 classes of chemicals, covering 11 typical volatile compound species, were selected for initial calibration. Over four months, experimental data were collected under stringent operational controls. Finally, Silhouette coefficients were utilized to evaluate the difference among the 11 chemical categories. The calibration chemicals selection method we proposed is generic and has instructive and reference value for the calibration of general-purposed E-noses.

II. Chemicals Selection Criteria For Calibration

Chemical industries, fuel combustion and pharmaceutical facilities are primary sources of chemicals. Among them, volatile substances are mainly concentrated in halogenated hydrocarbons, aldehydes, aromatic compounds, polycyclic aromatic hydrocarbons, alcohols, alkanes, ketones, olefins, and ethers [28]. However, not all chemicals would be acceptable as calibration chemicals. Ideally, we would like our test chemicals to fulfil the following criteria:

A. Universality

1) Applicable to the widest range of international standards, apparatus, and application contexts.
2) Common, easy to obtain and store.
3) Economic.

We considered these point from three perspectives: current international standards [27]-[32], public datasets [33]-[39], and published papers [40]-[46]. Finally, we retained the same selection of chemicals in various standards and settings and gathered 57 acceptable test chemicals to create an initial database [27].

B. Safety

Safety is also a vital factor. The selected chemicals must be non-toxic or less harmful and cause minimum environmental pollution. The 57 chemicals included in the database were further reduced, considering safety factor [27]. First, VOCs were divided into ten categories based on their functional groups: hydrocarbons, ketones, aldehydes, benzenes, amines, alcohols, ethers, hydroxy acids, ester, and halogenated hydrocarbons. Inorganic compounds were placed together into a single category.

Consequently, the initial calibration chemical database consisting of 57 chemicals were divided into eleven groups covering organic and inorganic compounds. The median lethal dose (LD_{50}) was then utilized as a safety indicator for chemical selection. Compounds with the lowest LD_{50} values in each category, such as carbonyl chloride (highly toxic), acrylonitrile (LD_{50} = 93 mg/kg), diborane (LD_{50} = 58 mg/kg) and ethylene oxide (LD_{50} = 72 mg/kg), were removed. The least toxic chemical of each category was retained (see Table I).

C. Sensibility

The selected chemicals must be capable of covering as many sensors as possible. Gas sensors have performance factors such as sensitivity, selectivity, reaction time, recovery time, and stability. We also selected chemicals considering their coverage on sensors, i.e., those chemicals with more robust sensor responses will be selected as calibration chemicals.

D. Differentiation

We selected chemicals with good distinguishing ability, which makes it easier to observe the direction of gas sensor drift and helps with compensation of sensor drift.

III. Methodology and Experimental Platform

The self-developed E-nose collected datasets for 4 months (See Fig. 1). In the dataset, eight features were extracted from each sensor's responses, including two steady-state features and six exponential moving average features (See Section IV, part A for details). The sample matrix is $\mathbf{X} = [\mathbf{x}_1, \mathbf{x}_2, \cdots, \mathbf{x}_i, \cdots, \mathbf{x}_m]^{\mathrm{T}}$, $\mathbf{x}_i$ represents the i-th sample, and $m = 210$ denotes the total number of samples in the dataset.

A. Signal Processing Method.

1) Principal Component Analysis [47]: Principal Component Analysis (PCA) is a standard method for reducing linear dimensions based on statistical analysis. The dimensionality of the original high-dimensional data is reduced through linear mapping. The objective is to make the distribution of the reduced-dimensional data on the axes as dispersed as feasible. To achieve this, the variance on the new coordinates must be maximized through the following:

$$\mathbf{w}^* = \underset{\|\mathbf{w}\|=1}{\operatorname{argmax}}(\mathbf{w}^{\mathrm{T}}\mathbf{X}^{\mathrm{T}}\mathbf{X}\mathbf{w}) \quad (1)$$

where it is assumed that the matrix $\mathbf{X}$ is mean-centered (then all

linear combinations are also mean-centered). The latter problem is a standard problem in linear algebra and the optimal $\mathbf{w}$ is the (standardized) first eigenvector (i.e. the eigenvector with the largest value) of the covariance matrix $\mathbf{X}^{\mathrm{T}}\mathbf{X}$.

2) Linear Discriminant Analysis [48]: LDA is a supervised learning algorithm. The data is projected in a low dimension using the dimensionality reduction technique. The projection points of each type of data are expected to be as close as possible. We can determine the category based on the position of the new sample projection point when classifying a new sample. This specific algorithm can be described as follows:

The total within-class scatter matrix $\mathbf{S}_\omega$ is:

$$\mathbf{S}_\omega = \sum_{j=1}^{K}\sum_{\mathbf{x}_i\in G_j}\left(\mathbf{x}_i-\boldsymbol{\mu}_j\right)\left(\mathbf{x}_i-\boldsymbol{\mu}_j\right)^{\mathrm{T}}, j = 1,2,\cdots K \quad (2)$$

where $\mathbf{S}_\omega$ is the sum of the covariance matrices of samples with unified label, the variance of the same sample after projection is as small as possible, so as these samples are as close as possible. $\boldsymbol{\mu}_j$ is the mean feature vector of samples in jth class. The number of known pattern classes is K, as ($G_1, G_2, \cdots, G_K$).

Between-class scatter matrix $\mathbf{S}_b$:

$$\mathbf{S}_b = \sum_{j=1}^{K}\left(\boldsymbol{\mu}_j-\boldsymbol{\mu}\right)\left(\boldsymbol{\mu}_j-\boldsymbol{\mu}\right)^{\mathrm{T}}, j = 1,2,\cdots K \quad (3)$$

where $\mathbf{S}_b$ is the covariance matrix of the mean of each class of sample, the sample projections between different classes are as far apart as possible to facilitate the reduction of data dimensionality. $\boldsymbol{\mu}$ is the mean feature vector of total samples.

The optimal projection direction can be found using the Fisher criterion function defined as:

$$\boldsymbol{\omega}^{*} = \underset{\boldsymbol{\omega}}{\operatorname{argmax}}\frac{\boldsymbol{\omega}^{\mathrm{T}}\mathbf{S}_b\boldsymbol{\omega}}{\boldsymbol{\omega}^{\mathrm{T}}\mathbf{S}_\omega\boldsymbol{\omega}} \quad (4)$$

In Eq. (4), the between class and within-class ration can be considered a comprehensive measure. It determines the data separability after projection. When the full separability measure reaches the maximum, the Fisher optimal projection direction is determined.

B. Quantification of sample variation by Silhouette coefficient [49]

To quantify the separability of samples, the Silhouette coefficient was used. The formula for calculating the Silhouette coefficient is as follows:

$$s(i) = \frac{b(i)-a(i)}{max\{a(i),b(i)\}} \quad (5)$$

$$a(i) = \frac{1}{|C_I|-1}\sum_{j\in C_I, i\neq j} d(i,j) \quad (6)$$

where $a(i)$ represents the cohesiveness of the sample points and denotes the average distance among i and other points in the same cluster. Let $|C_I|$ be the number of points belonging to cluster I, and $d(i,j)$ denotes the distance among points i and $j\ in\ C_I$.

The calculation of $b(i)$ is similar to that of $a(i)$ and represents the average distance from point i to all points in another most adjacent cluster.

$$b(i) = \min_{J\neq I}\frac{1}{|C_J|}\sum_{j\in C_J} d(i,j) \quad (7)$$

In summary, $s(i)$ is calculated as follows.

$$s(i) = \begin{cases} 1-\frac{a(i)}{b(i)}, & a(i) < b(i) \\ 0, & a(i) = b(i) \\ \frac{b(i)}{a(i)}-1, & a(i) > b(i) \end{cases} \quad (8)$$

From equation (8) it can be seen that:
when $a(i) < b(i)$, the distance within a cluster is smaller than the distance between the two clusters, and the clustering result is more compact. The more the value of $s(i)$ approaches 1 the better the clustering effect.

Conversely, when $a(i) > b(i)$, the distance within a cluster is greater than the distance between clusters. The more the value of $s(i)$ approaches -1, the worse the clustering effect is.

C. Observation of sensor drift

The sensor response is defined as follows [50]:

$$S = \frac{R_g-R_a}{R_a} \quad (9)$$

where R_a is the resistance of the sensor in pure air and R_g is its resistance in the appearance of chemical to be tested.

D. Experimental E-nose system

The self-developed E-nose contained the sensor array listed in Table II. To reduce the impact of temperature, all metal oxide sensors (MOS) were placed in a thermostatically heated gas chamber.

The remaining sensors were put in a second gas chamber at ambient temperature. The above gas chambers were coupled to a self-developed automatic sampling module [51] and the test chemicals were provided through collection bags. The system is automatically controlled by a computer built into the E-nose to switch among multiple inlet gas pathways [52]. Fig. 1 shows the schematic of the E-nose system (Here, the Tablet PC, I/O control module, and Power supply module are all built into the E-nose except the Solenoid valves T1 and T2).

We defined a protocol for these experiments that allowed for the testing of multiple chemicals at different concentrations. In all these experiments, zero air was used as the carrier gas [52]. The sensors were exposed to the 14 chemicals in a random order, with this order being randomized with each set of experiments. Each sample collection process consists of four distinct phases.

1) Cleaning phase (P1): Zero air is flowed through the system to clean the unit before use.
2) Baseline phase (P2): Flow rate changed to match measurement phase, and the baseline steady-state sensor responses were collected.
3) Injection phase (P3): The test chemical was injected into the gas chamber through an automatic sample injection module.
4) Purging phase (P4): The E-nose is purged with zero air.

The total acquisition time of the experiment is 24 minutes, including 2 minutes for P1, 1 minute for P2, 6 minutes for P3,

and 15 minutes for P4, with the sampling rate being 1 Hz.

The gas flow rate was set to 40 mL/min for P2 and P3, 500 mL/min for P1 and P4. The sensors were preheated for seven days before the start of the first experiment, and all sensors were operated in line with manufacturers specifications. According to our previous study [35], the gas flow rates of our E-nose were optimized by air chamber airflow simulation and experiments. The optimized airflow rate can sufficiently make the sensor array of the E-nose react with chemicals in the air chamber.

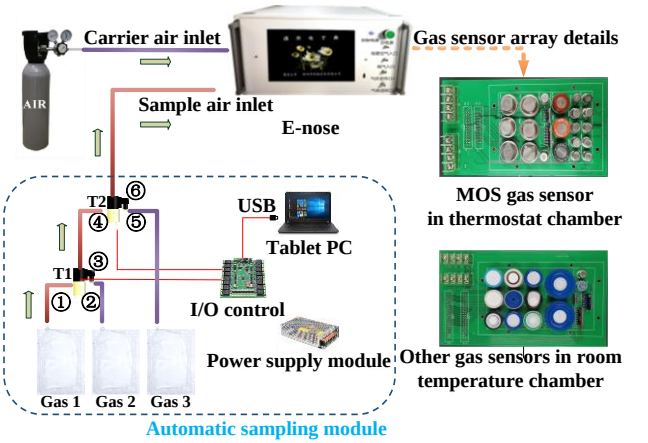

(a)

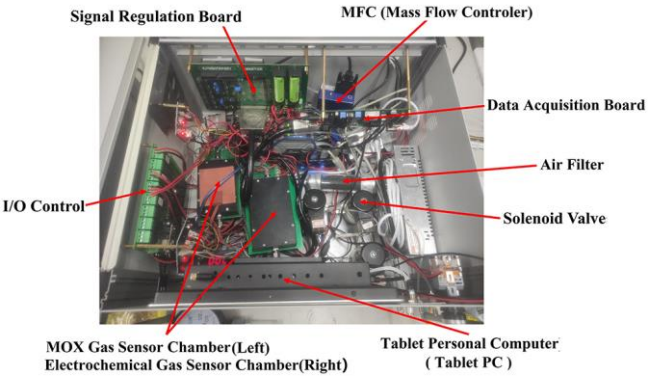

(b)

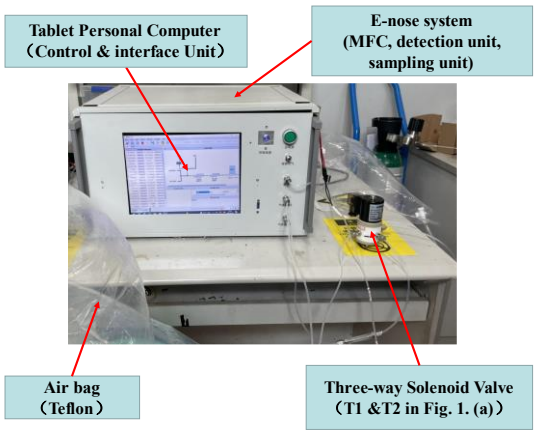

(c)

Fig. 1. Our E-nose system (a) Structural diagram (b) Photo of its interior (c) Photo of the whole system

E. Target chemicals

These chemicals should guarantee the reproducibility of the protocol in different laboratories and with different instruments. Table I provides information on the 14 chemicals. It is worth noting that the 14 chemicals included in Table I cover ten major categories of common volatile and inorganic compounds. The detailed selection procedure for chemicals is described in Section II. In addition, the CAS number of each chemical is given in column 3 of Table I. Column 5 of Table I give the LD_{50} for each chemical.

TABLE I
DETAILS ABOUT TARGET CHEMICALS

No.	Analytes	CAS [27]	Category	LD_{50} [29]	Concentration (ppm)
1	N-hexane	110-54-3	Hydrocarbons	25000	30, 50, 100
2	Acetone	67-64-1	Ketones	5800	30, 50, 100
3	Acetaldehyde	75-07-0	Aldehydes	1930	30, 50, 100
4	Formaldehyde	50-00-0	Aldehydes	800	30, 50, 100
5	Toluene	108-88-3	Benzene	5000	30, 50, 100
6	Benzene	71-43-2	Benzene	3306	30, 50, 100
7	N-butylamine	109-73-9	Amines	366	30, 50, 100
8	Ethanol	64-17-5	Alcohols	7060	30, 50, 100
9	Isopropanol	67-63-0	Alcohols	5840	30, 50, 100
10	Tetrahydrofuran	109-99-9	Ether	1650	30, 50, 100
11	Acetic acid	64-19-7	Hydroxy acids	3300	30, 50, 100
12	Ethyl acetate	141-78-6	Lipids	5620	30, 50, 100
13	Tetrachloroethene	127-18-4	Halocarbons	3005	30, 50, 100
14	Ammonia	7664-41-7	Inorganic compounds	350	30, 50, 100

Note: the LD_{50} is an indicator describing the toxicity of a toxic substance or radiation; it indicates the minimum number of bacteria or amount of toxin required to kill half an animal of certain body weight or age via a specified route of infection in a specific time [29]. Higher LD_{50} means lower toxicity for the corresponding chemical.

TABLE II
INFORMATION OF THE GAS SENSORS

No.	Sensor	Type	Manufacturer (Country)	No.	Sensor	Type	Manufacturer (Country)
1	TGS813	MOS	Figaro (Japan)	22	ME4-H2S	Electrochemical	Winsen (China)
2	TGS2610D	MOS	Figaro (Japan)	23	NH3-3E100SE	Electrochemical	City (UK)
3	MS1100	MOS	Ogam (Korea)	24	4-CH3SH-10	Electrochemical	Solidsense (GER)
4	TGS826	MOS	Figaro (Japan)	25	SMD1013	MEMS	Huimin Tech. (China)
5	TGS2602	MOS	Figaro (Japan)	26	SMD1001	MEMS	Huimin Tech. (China)
6	TGS822	MOS	Figaro (Japan)	27	MQ135	MOS	Winsen (China)
7	MG812	Solid electrolytes	Winsen (China)	28	MP503	MOS	Winsen (China)
8	4S	Electrochemistry	City (UK)	29	MQ3B	MOS	Winsen (China)
9	4HS+	Electrochemical	City (UK)	30	MQ137	MOS	Winsen (China)
10	ME4-C6H6	Electrochemical	Winsen (China)	31	4ETO-10	Electrochemical	Honeywell (USA)
11	SMD1007	MEMS	Huimin Tech. (China)	32	4OXV	Electrochemical	City (UK)
12	WSP2110	MOS	Winsen (China)	33	MQ138	MOS	Winsen (China)
13	MP4	MOS	Winsen (China)	34	MP901	MOS	Winsen (China)
14	MP135A	MOS	Winsen (China)	35	ME3-C2H6S	Electrochemical	Winsen (China)
15	TGS2620	MOS	Figaro (Japan)	36	ME3-CH2O	Electrochemical	Winsen (China)
16	TGS2611E	MOS	Figaro (Japan)	37	PID-AH	Photo-ionization	Alphasense (UK)
17	AQ201	MOS	FIS (Japan)	38	DHT95	Temperature & humidity	Senrisirion (CH)
18	TGS8669	MOS	Figaro (Japan)	39	DHT95	Temperature & humidity	Senrisirion (CH)
19	2M012	Semi-conductors	Guotai Hengan (China)	40	GY63	Air pressure	MEAS (USA)
20	TGS2600	MOS	Figaro (Japan)	41	GY63	Air pressure	MEAS (USA)
21	MR516	Hot line	Winsen (China)	/	/	/	/

IV. RESULTS AND DISCUSSION

The entire calibration chemical screening process is summarized in Fig. 2.

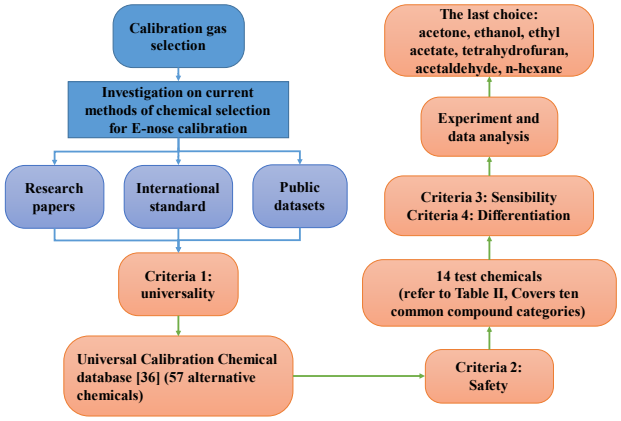

Fig. 2. E-nose calibration chemical selection flow chart.

A. Dataset description

The dataset was created from using 14 chemicals at 3 concentrations. For each response curve, eight features were extracted, including two steady-state features and six exponential moving average features. The two steady-state features used were the difference of the maximal resistance change and the baseline, and its normalized version expressed by the ratio of the maximal resistance and the baseline values. For the sensor dynamics, the increasing/decaying transient portion of the sensor response (P3) was used. Further information on feature extraction can be found in [19]. Therefore, a dimensional feature vector for each observation was created. This process was repeated twice at different time intervals. Therefore, the dataset consisted of 14 chemicals, three concentrations for each chemical, and five repeated experiments (a total of 210 samples × 2 batches). This study did not consider complex mixtures, and the test conditions were strictly maintained during this period.

B. Sensitivity analysis of sensor arrays

Responses of the sensors to the 14 different chemicals are shown in Table III. Experiments for each chemical were performed on the same day to eliminate sensor drift caused by temporal variations. A higher response value means the sensor responded more "strongly" to that chemical. Here the "Response" column in Table III denotes the average of responses to a chemical for all sensors of the sensor array.

TABLE III
RESPONSES OF THE SENSOR ARRAY

Rank	Chemicals	Response	Sensor coverage (%)
1	Ethyl acetate	6.77	83%
2	Acetone	6.69	78%
3	Ethanol	6.63	83%
4	Tetrahydrofuran	6.00	83%
5	Acetaldehyde	5.93	83%
6	Isopropanol	4.72	85%
7	Toluene	3.88	76%
8	Benzene	3.44	83%
9	N-hexane	2.93	76%
10	Ammonia	2.25	63%
11	Acetic acid	2.22	63%
12	Formaldehyde	1.57	66%
13	Tetrachloroethene	1.28	41%
14	N-butylamine	1.11	44%

We can use this metric to determine which chemicals cover a more comprehensive range of sensors and rank them from the

highest to lowest sensor response value. According to the data in the "Sensor coverage" column in Table III, ethyl acetate, acetone, and ethanol are the three chemicals to which the sensor array responds most strongly. In contrast, the sensor array responds the least to tetrachloroethylene and n-butylamine, which also have the lowest sensor coverage. The two evaluation indicators, sensor response value and coverage, make it easy to select calibration chemicals. It is worth noting that the central point is to select compounds for E-nose calibration from a wide range of chemicals rather than considering the cross-sensitivity of the E-nose system. From the calibration perspective, sensor specificity increases the difficulty of calibration. Therefore, selecting chemicals with higher sensitivity and broader sensor coverage facilitates drift observation and calibration.

C. Qualitative result of chemicals differentiation

Principal component analysis (PCA) was applied to the dataset to observe the collected feature of dataset distribution changes with time. Fig. 3 shows the PCA result for the 14 chemicals. In Fig. 3, different colored dots represent different kinds of chemical samples.

Maintaining a minimum intra-class distance among samples and a maximum inter-class distance constitutes our screening criteria for chemical differentiation. As shown in the red boxes in Fig. 3, n-butylamine, acetic acid, formaldehyde, n-hexane, and benzene are mixed. Each chemical has three concentrations, which is one of the reasons why some chemicals cannot be separated. Furthermore, the large number of sensors and sample features lead to the low contribution of the first two dimensions of the PCA, as shown in Fig. 3.

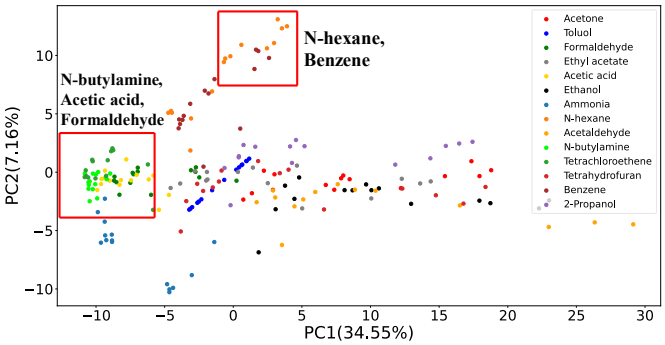

Fig. 3. PCA plot for data from the 14 chemicals (before drift, batch 1).

To observe the differences in the distributions of samples, a linear discriminant analysis (LDA) algorithm was applied to the dataset, as shown in the red box in Fig. 4. Almost all chemicals are differentiable except n-butylamine and formaldehyde.

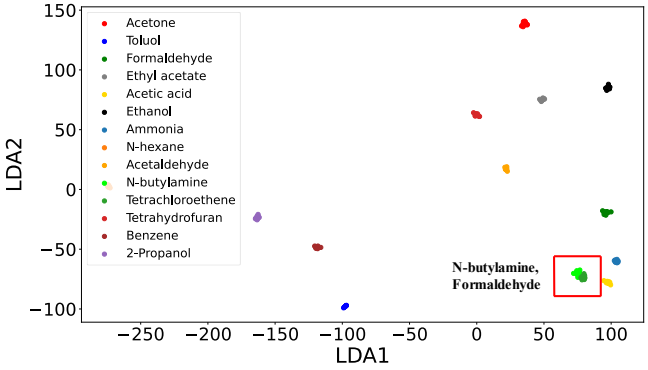

Fig. 4. LDA result of data collected from 14 chemicals (before drift, batch 1).

We then used the Silhouette coefficient to give a score to the E-nose's ability to differentiate the test chemicals. Generally, Silhouette coefficients are applied to clustering methods and mostly to unsupervised approaches. However, calculating the Silhouette coefficient after the clustering, such as K-means, can result in misclassification and give an incorrect overall score. Fig. 5 shows the Silhouette coefficients of each category after the data are clustered by K-means (k=14).

Due to the misclassification of K-means clustering, the number of samples in each category is unequal, and the overall Silhouette coefficient reaches 0.117, shown as a dotted line in Fig. 5. The Silhouette coefficient reaches 0.165 with k=8 being the optimal number of clusters determined by the K-means clustering algorithm.

To solve the problem, it is necessary to introduce accurate sample labels to ensure the accuracy of the clustering/classification. With two minor modifications, we can still use the Silhouette coefficient method.

1) Since we know the exact class and number of chemicals, we no longer use K-means to find the optimal K-values; instead, we fix k (which is equal to the exact number of chemicals we tested) and calculate their Silhouette coefficients.
2) Use the original data or the data resulting from the LDA.

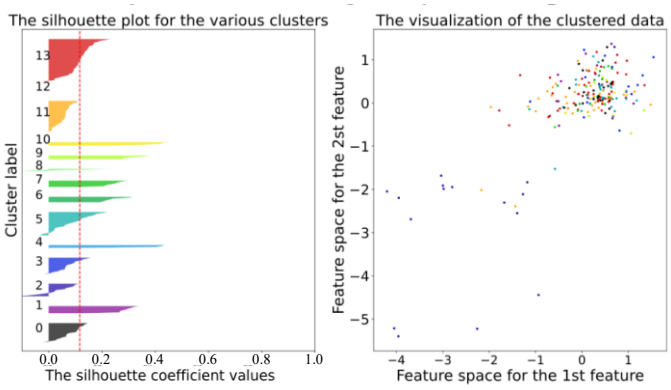

Fig. 5. Silhouette values calculated after K-means (k=14) (before drift, batch 1).

First, the data were analyzed using LDA or original, explicitly given the labels of all points. The algorithm will

classify the points according to their true labels. Then, Silhouette coefficients are introduced to measure the clarity of the contours of each category. The distinctions of the 14 chemicals initially selected in Table I are quantified, and the results are shown in Fig. 6.

The right side of Fig. 6(a) shows the original data 2-D visualization of all the samples in Table I, the left side shows the Silhouette coefficients of samples, and the dashed lines represent the average Silhouette coefficients for all samples. It can be seen from Fig. 6(a) that the uneven distribution of samples caused by the misjudgment of the clustering method can be improved by introducing the true labels. Fig. 6(b) shows the LDA result of all the samples in Table I. The Silhouette coefficient is raised to 0.94 (dotted line in Fig. 6(b)). Since all samples are given label information, the number of all sample categories in the figure is equal. After adjustment, we describe the variability among chemical substances with a single parameter, with the Silhouette coefficients being an efficient means to achieve this.

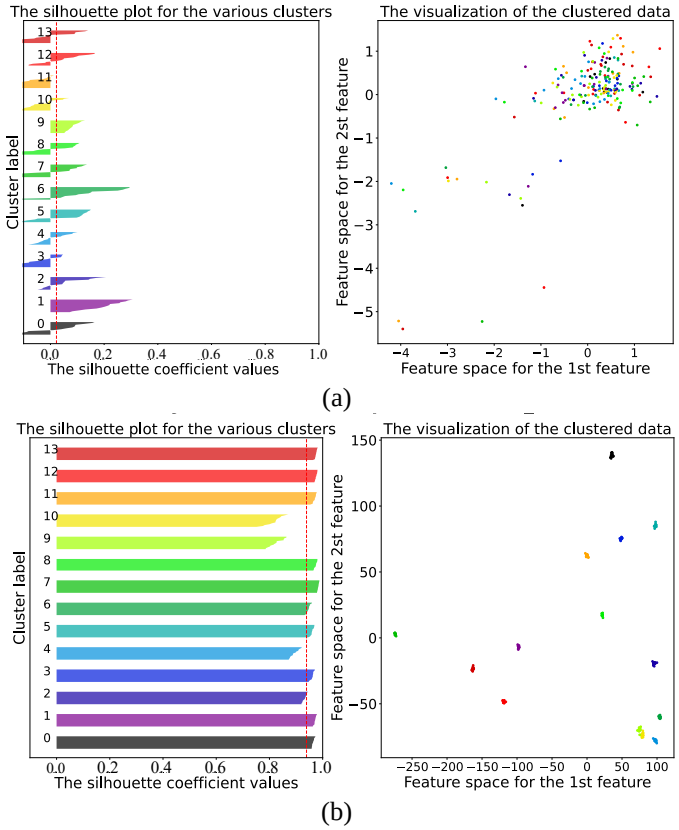

Fig. 6. Silhouette values and the visualization of data (no clustering method used, before drift, batch 1). (a) original data. (b) after LDA.

Furthermore, Fig. 6 demonstrates that the Silhouette coefficients of n-butylamine, formaldehyde, and acetic acid are less than the average Silhouette coefficients of 0.94, which means that three samples are mixed. This calculated result is similar to what is observed in Fig. 4, indicating that the discrimination performance of n-butylamine, formaldehyde, and acetic acid is worse than that of other chemicals. Therefore n-butylamine, formaldehyde, and acetic acid can be excluded in priority from the consideration of the differentiation criterion.

D. Drift resistance of chemicals

To reduce the scale variants among dimensions, the whitening processing (centralization) was conducted on the data. To visually observe the drift of the heterogeneous E-nose data, we have plotted the LDA scatter points in Fig. 7, in which Fig. 7(a) is calculated on the raw data of batch 1 (before drift), and Fig. 7(b) is calculated on the raw data of batch 2 (after drift). From Fig. 7, it is clear that the low-dimensional subspace between batch 1 and batch 2 is significantly biased (inconsistent) due to drift over time.

We applied an LDA to analyze the drift of data samples, using red boxes to highlight the parts of the samples that overlap. Comparing the sample distribution before and after the drift, the drift resulting from the chemicals can be observed. Ideally, we are after chemicals that result in large drifts over time as these are more useful for E-nose calibration. As shown in Fig. 7(b), formaldehyde and n-butylamine still overlap after drift. However, this drift does not affect their relative positions.

The “Response” column in Table III indicates that the response for formaldehyde and n-butylamine are low, with values of 1.57 and 1.11 respectively. This ranks then at the bottom. In addition, their sensor coverage is also low. Therefore, stable and non-time-varying chemicals are not effective in observing changes in the sensor response, which is detrimental to E-nose calibration. Fig. 7 showed that acetic acid, ethanol, and tetrahydrofuran met the requirements and could be used as calibration chemicals.

In summary, the least toxic chemicals in each category were first selected from the calibration database (see Table I). Then, the chemicals in Table III that were ranked low in both response and sensor coverage, such as formaldehyde, tetrachloroethene, and n-butylamine, were removed. Next, Fig. 6 shows that the Silhouette coefficients of n-butylamine, formaldehyde, and acetic acid were less than the average Silhouette coefficients of 0.94, indicating the identification performance of n-butylamine, formaldehyde, and acetic acid was worse than other chemicals. Therefore n-butylamine, formaldehyde, and acetic acid were excluded. Since both formaldehyde and acetaldehyde are all aldehydes, while the later has superior sensibility and differentiation, we only kept acetaldehyde. Figure 7 shows that acetic acid, ethanol, and tetrahydrofuran meet the requirements and could be used as calibration chemicals. Finally, we selected acetone, ethanol, ethyl acetate, tetrahydrofuran, acetaldehyde, and n-hexane as the top six calibration chemicals.

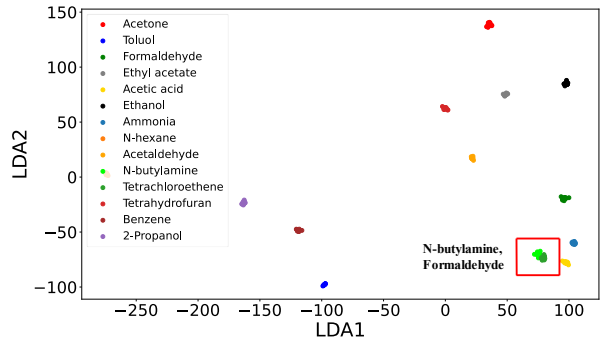

(a)

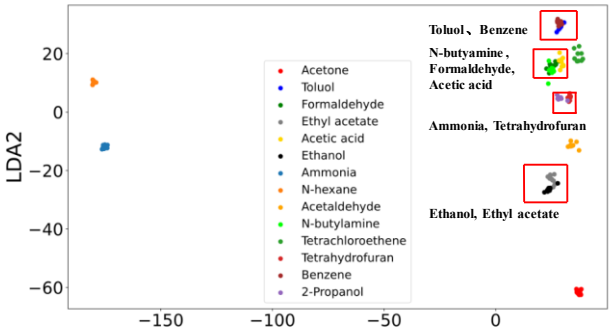

(b)

Fig. 7. Distribution of 14 chemical samples. (a) batch 1 (before drift). (b) batch 2 (after drift).

V. Conclusion

In this paper, we proposed a method of chemical selection based on a number of selection criteria. To find the most representative chemicals for calibration of a general-purposed E-nose, we investigated the sources and compositions of volatile compounds in various environments/documents, and identified six chemicals: acetone (ketone), ethanol (alcohol), ethyl acetate (ester), tetrahydrofuran (ether), acetaldehyde (aldehyde), and n-hexane (alkane) based on the four criteria (universality, safety, sensibility and differentiation) combined with the Silhouette coefficients from laboratory experiments.

The method of selecting calibration chemical proposed here is generic and will have use for general-purpose E-noses. In the future, we will do experiments over longer periods of time to further investigate the lifetime and drift of E-noses. However, beyond considering the safety factor, our method has not been verified in detecting higher toxic / harmful chemicals, so further studies on these chemicals will also be needed.

Acknowledgment

The authors would like to acknowledge the National Natural Science Foundation of China (62171066) for its fund support.

References

[1] J. Qian, M. Lu, F. Tian, and R. Liu, "Study on Sensor Array Optimization of Medical Electronic Nose for Wound Infection Detection," *IEEE Transactions on Circuits and Systems II: Express Briefs*, vol. 69, no. 3, pp. 1867-1871, 2022.

[2] J. L. Herrero *et al*., "A web-based approach for classifying environmental pollutants using portable E-nose devices," *IEEE Intell. Syst.*, vol. 31, no. 3, pp. 108-112, May. 2016.

[3] Q. Li, Y. Gu, and N.-f. Wang, "Application of Random Forest Classifier by Means of a QCM-Based E-Nose in the Identification of Chinese Liquor Flavors," *IEEE Sensors Journal*, vol. 17, no. 6, pp. 1788-1794, 2017.

[4] D. Galvan, A. Aquino, L. Effting, A. C. G. Mantovani, E. Bona, and C. A. Conte-Junior, "E-sensing and nanoscale-sensing devices associated with data processing algorithms applied to food quality control: a systematic review," *Crit Rev Food Sci Nutr*, vol. 62, no. 24, pp. 6605-6645, 2022.

[5] D. Luo *et al*., "Aroma characteristic analysis of Amomi fructus from different habitats using machine olfactory and gas chromatography-mass spectrometry," *Pharmacognosy Magazine*, vol. 15, no. 63, 2019.

[6] D. Terutsuki, T. Uchida, C. Fukui, Y. Sukekawa, Y. Okamoto, and R. Kanzaki, "Real-time odor concentration and direction recognition for efficient odor source localization using a small bio-hybrid drone," *Sensors and Actuators B: Chemical*, vol. 339, 2021.

[7] H. Holmberg *et al*., "Drift counteraction for an electronic nose," *Sensors and Actuators B: Chemical*, vol. 36, no. 1-3, pp. 528-535, Oct. 1996.

[8] S. Deshmukh, R. Bandyopadhyay, N. Bhattacharyya, R. A. Pandey, and A. Jana, "Application of electronic nose for industrial odors and gaseous emissions measurement and monitoring--An overview," *Talanta*, vol. 144, pp. 329-40, Nov 1 2015.

[9] A. Hierlemann and R. Gutierrez-Osuna, "Higher-order chemical sensing," *ACS Chem.*, vol. 108, no. 2, pp. 563-613, Jan. 2008.

[10] B.-Y. Kim *et al*., "Extremely sensitive ethanol sensor using Pt-doped SnO2 hollow nanospheres prepared by Kirkendall diffusion," *Sensors and Actuators B: Chemical*, vol. 234, pp. 353-360, 2016.

[11] A. Vergara *et al*., "Quantitative gas mixture analysis using temperature-modulated micro-hotplate gas sensors: Selection and validation of the optimal modulating frequencies," *Sensors and Actuators B: Chemical*, vol. 123, no. 2, pp. 1002-1016, 2007.

[12] S. Marco and A. Gutierrez-Galvez, "Signal and Data Processing for Machine Olfaction and Chemical Sensing: A Review," *IEEE Sensors Journal*, vol. 12, no. 11, pp. 3189-3214, 2012.

[13] H. Wang, Z. Zhao, Z. Wang, G. Xu, and L. Wang, "Independent Component Analysis-Based Baseline Drift Interference Suppression of Portable Spectrometer for Optical Electronic Nose of Internet of Things," *IEEE Transactions on Industrial Informatics*, vol. 16, no. 4, pp. 2698-2706, 2020.

[14] S. Arunachalam, R. Izquierdo, and F. Nabki, "Ionization Gas Sensor using Suspended Carbon Nanotube Beams," *Sensors (Basel)*, vol. 20, no. 6, Mar 17 2020.

[15] M. Padilla, A. Perera, I. Montoliu, A. Chaudry, K. Persaud, and S. Marco, "Drift compensation of gas sensor array data by Orthogonal Signal Correction," *Chemometrics and Intelligent Laboratory Systems*, vol. 100, no. 1, pp. 28-35, 2010.

[16] Z. Yi and C. Li, "Anti-Drift in Electronic Nose via Dimensionality Reduction: A Discriminative Subspace Projection Approach," *IEEE Access*, vol. 7, pp. 170087-170095, 2019.

[17] A. u. Rehman and A. Bermak, "Heuristic Random Forests (HRF) for Drift Compensation in Electronic Nose Applications," *IEEE Sensors Journal*, vol. 19, no. 4, pp. 1443-1453, 2019.

[18] L. Zhang and D. Zhang, "Efficient Solutions for Discreteness, Drift, and Disturbance (3D) in Electronic Olfaction," *IEEE Transactions on Systems, Man, and Cybernetics: Systems*, vol. 48, no. 2, pp. 242-254, 2018.

[19] A. Vergara, S. Vembu, T. Ayhan, M. A. Ryan, M. L. Homer, and R. Huerta, "Chemical gas sensor drift compensation using classifier ensembles," *Sensors and Actuators B: Chemical*, vol. 166-167, pp. 320-329, 2012.

[20] H. Wang *et al*., "Unsupervised Cross-User Adaptation in Taste Sensation Recognition Based on Surface Electromyography," *IEEE Transactions on Instrumentation and Measurement*, vol. 71, pp. 1-11, 2022.

[21] Y. Tao, H. C. Yang, Z. F. Laing, "Sensor Online Drift Compensation Algorithm Based on Subspace Distribution Adaptive," *new generation information technology*, vol. 24, no. 5, pp. 2-9, Aug. 2019.

[22] Z. Liang *et al*., "A novel WWH problem-based semi-supervised online method for sensor drift compensation in E-nose," *Sensors and Actuators B: Chemical*, vol. 349, 2021.

[23] Z. Lei and D. Zhang, "Domain Adaptation Extreme Learning Machines for Drift Compensation in E-Nose Systems," *IEEE Transactions on Instrumentation and Measurement*, vol. 64, no. 7, pp. 1790-1801, 2015.

[24] J. Burgues, J. M. Jimenez-Soto, and S. Marco, "Estimation of the limit of detection in semiconductor gas sensors through linearized calibration models," *Anal Chim Acta*, vol. 1013, pp. 13-25, Jul 12 2018.

[25]M. Padilla, A. Perera, I. Montoliu, A. Chaudry, K. Persaud, and S. Marco, "Drift compensation of gas sensor array data by Orthogonal Signal Correction," *Chemometrics and Intelligent Laboratory Systems*, vol. 100, no. 1, pp. 28-35, 2010.
[26]T. Artursson, "Drift correction for gas sensors using multivariate methods," *John Wiley and Sons, Ltd.*, vol. 14, no. 5-6, pp. 711-723, Sep. 2000.
[27]Multigas Sensors- Function, Classification and Assessment, DE-VDI Standard VDI/VDE 3518, 2018.
[28]Workplace atmospheres- Electrical apparatus used for the direct detection and direct concentration measurement of toxic gases and vapours. General requirements and test methods, BSI Standard BS EN 45544, 2016.
[29]Niosh pocket guide to chemical hazards, DHHS(NIOSH) Standard, 2005.
[30]Sensory analysis- Methodology- "A"- "not A" test, ISO/TC Standard ISO 8588: 2017, 2017.
[31]Sensor analysis-Methodology- Paired comparison test, ISO/TC Standard ISO 5495: 2005, 2005.
[32]Steel wire and wire products- Non-ferrous metallic coatings on steel wire, CSN Standard EN 10244-2, 2009.
[33]J. Fonollosa, I. Rodriguez-Lujan, M. Trincavelli, A. Vergara, and R. Huerta, "Chemical discrimination in turbulent gas mixtures with MOX sensors validated by gas chromatography-mass spectrometry," *Sensors (Basel)*, vol. 14, no. 10, pp. 19336-53, Oct 16 2014.
[34]J. Fonollosa, S. Sheik, R. Huerta, and S. Marco, "Reservoir computing compensates slow response of chemosensor arrays exposed to fast varying gas concentrations in continuous monitoring," *Sensors and Actuators B: Chemical*, vol. 215, pp. 618-629, 2015.
[35]A. Ziyatdinov, J. Fonollosa, L. Fernández, A. Gutierrez-Gálvez, S. Marco, and A. Perera, "Bioinspired early detection through gas flow modulation in chemo-sensory systems," *Sensors and Actuators B: Chemical*, vol. 206, pp. 538-547, 2015.
[36]J. Burgues and S. Marco, "Multivariate estimation of the limit of detection by orthogonal partial least squares in temperature-modulated MOX sensors," *Anal Chim Acta*, vol. 1019, pp. 49-64, Aug 17 2018.
[37]I. Rodriguez-Lujan, J. Fonollosa, A. Vergara, M. Homer, and R. Huerta, "On the calibration of sensor arrays for pattern recognition using the minimal number of experiments," *Chemometrics and Intelligent Laboratory Systems*, vol. 130, pp. 123-134, 2014.
[38]A. Vergara, J. Fonollosa, J. Mahiques, M. Trincavelli, N. Rulkov, and R. Huerta, "On the performance of gas sensor arrays in open sampling systems using Inhibitory Support Vector Machines," *Sensors and Actuators B: Chemical*, vol. 185, pp. 462-477, 2013.
[39]R. Huerta, T. Mosqueiro, J. Fonollosa, N. F. Rulkov, and I. Rodriguez-Lujan, "Online decorrelation of humidity and temperature in chemical sensors for continuous monitoring," *Chemometrics and Intelligent Laboratory Systems*, vol. 157, pp. 169-176, 2016.
[40]H. Liu, Q. Li, and Y. Gu, "A multi-task learning framework for gas detection and concentration estimation," *Neurocomputing*, vol. 416, pp. 28-37, 2020.
[41]L. Fernandez, J. Yan, J. Fonollosa, J. Burgues, A. Gutierrez, and S. Marco, "A Practical Method to Estimate the Resolving Power of a Chemical Sensor Array: Application to Feature Selection," *Front Chem*, vol. 6, p. 209, 2018.
[42]K. Yan, L. Kou, and D. Zhang, "Learning Domain-Invariant Subspace Using Domain Features and Independence Maximization," *IEEE Trans Cybern*, vol. 48, no. 1, pp. 288-299, Jan 2018.
[43]Y. Tao, *et al*., "Domain Correction Based on Kernel Transformation for Drift Compensation in the E-Nose System," *Sensors*, vol. 18, no. 10, pp. 3209, Oct. 2018.
[44]Y. Tao, J. Xu, Z. Liang, L. Xiong, and H. Yang, "Domain Correction Based on Kernel Transformation for Drift Compensation in the E-Nose System," *Sensors (Basel)*, vol. 18, no. 10, Sep 23 2018.
[45]Y. Tao, C. Li, Z. Liang, H. Yang, and J. Xu, "Wasserstein Distance Learns Domain Invariant Feature Representations for Drift Compensation of E-Nose," *Sensors (Basel)*, vol. 19, no. 17, Aug 26 2019.
[46]A. Vergara, J. Fonollosa, J. Mahiques, M. Trincavelli, N. Rulkov, and R. Huerta, "On the performance of gas sensor arrays in open sampling systems using Inhibitory Support Vector Machines," *Sensors and Actuators B: Chemical*, vol. 185, pp. 462-477, 2013.
[47]M. Bari and W. B. Kindzierski, "Ambient volatile organic compounds (VOCs) in Calgary, Alberta: Sources and screening health risk assessment," *Science of The Total Environment*, vol. 631-632, no. 1, pp. 627-640, Aug. 2018.
[48]H. Chen, D. Huo, and J. Zhang, "Gas Recognition in E-Nose System: A Review," *IEEE Trans Biomed Circuits Syst*, vol. 16, no. 2, pp. 169-184, Apr 2022.
[49]X. Pan, X. Zhao, W. Xu, Z. Fan, and A. Bermak, "Programmable Nanoarchitectonics of Pore Array for Electronic-Nose-Based Early Disease Diagnose," *IEEE Transactions on Electron Devices*, vol. 69, no. 8, pp. 4514-4520, 2022.
[50]A. Et-taleby, *et al*., "Faults Detection for Photovoltaic Field Based on K-Means, Elbow, and Average Silhouette Techniques through the Segmentation of a Thermal Image," *International Journal of Photoenergy*, vol. 2020, no. 3, pp. 1-7, Nov. 2020.
[51]H. Ji, W. Zeng, and Y. Li, "Gas sensing mechanisms of metal oxide semiconductors: a focus review," *Nanoscale*, vol. 11, no. 47, pp. 22664-22684, Dec 21 2019.
[52]J. Qian, A. Zhang, F. Tian, and Y. Zhang, "A Pre-Concentration System Design for Electronic Nose via Finite Element Method," *IEEE Transactions on Circuits and Systems II: Express Briefs*, vol. 68, no. 12, pp. 3592-3596, 2021.
[53]S. Zhang *et al*., "A Universal Calibration Method for Electronic Nose Based on Projection on to Convex Sets," *IEEE Transactions on Instrumentation and Measurement*, vol. 70, pp. 1-12, 2021.
[54]J. Qian, Y. Luo, F. Tian, R. Liu, and T. Yang, "Design of Multisensor Electronic Nose Based on Conformal Sensor Chamber," *IEEE Transactions on Industrial Electronics*, vol. 68, no. 7, pp. 6276-6285, 2021.

Zhiyuan Wu received the master's degree in biochemistry and molecular biology from Fuzhou University, Fuzhou, China, in 2020. He is currently pursuing the Ph.D. degree with Chongqing University, Chongqing, China. His main research interests include, gas sensing techniques, and signal information processing.

Fengchun Tian received his B.Sc., M.Sc., and Ph.D. degrees in radio engineering, biomedical instruments and engineering, theoretical electric engineering from Chongqing University, Chongqing, P.R. China, in 1984, 1986, and 1996, respectively. Since 1984, he has been working in Chongqing University as a teacher. Since 2001, he has been a professor at Chongqing University. Currently, he is the director of Chongqing Key Laboratory of Bio-perception & Intelligent Information Processing. His research interests are artificial olfaction (E-nose) and modern signal processing technology.

James A. Covington (M'16) received the B.Eng. (Hons.) degree in electronic engineering and the Ph.D. degree from Warwick University in 1996 and 2000, respectively. His Ph.D. dissertation was on the development of CMOS and silicon-on-insulator CMOS gas sensors for room temperature and high-temperature operation. He was a Research Fellow with Warwick University and Cambridge University, on the development of gas and chemical sensors. He became a Lecturer at the School of Engineering, The University of Warwick, in 2002, and promoted to an Associate Professor in 2006, where he is currently a Professor of Electronic Engineering and the Head of the BioMedical Sensors Laboratory, School of Engineering. He has authored or co-

authored over 160 journal articles and patents. His current research interests focus on the development of microanalysis systems, E-noses, and ratification olfaction, employing a range of novel sensing materials, device structures, and microfabrication methods for applications with the environmental and medical application domains. More recently, based on his experience in gas sensing, he applied these skills in developing olfactory displays and related aroma-based technologies.

Hantao Li received his Master's degree in control engineering in 2020 from Chongqing University of Posts and Telecommunications, China. Since September 2020, he is currently pursuing a Ph.D. degree in Chongqing University. His research interests include E-nose and intelligent algorithm.

Siyuan Deng received the bachelor's degree in communication and engineering from Chongqing University, Chongqing, China, in 2022. He is currently persuing the master's degree with Chongqing University, Chongqing, China. His main research interests include E-nose machine learning, and signal information processing.